Abstract
This paper presents the experimental validation of a quasi-2D radial turbine model able to be used in turbocharged reciprocating internal combustion engine simulations. A passenger car VGT-type turbine has been tested under steady and pulsating flow conditions, instrumented with multiple pressure probes, temperature sensors, and mass flow sensors. Using the data obtained, a pressure decomposition has been performed. The pressure at the turbine inlet and outlet has been split into forward and backward travelling waves, employing the reflected and transmitted waves to verify the goodness of the model. The experimental results have been used to compare the quasi-2D radial turbine model as well as a classic 1D model. The quasi-2D code presents a good degree of correlation with the experimental results, providing better results than the one-dimensional approach, especially when studying the high frequency spectrum.

Keywords
Turbocharger, Mean-line model, Radial turbine simulation, Pulsating flow, Turbine 1D model

Introduction

Roughly one third of the energy released during the combustion phase in an reciprocating internal combustion engine (ICE) escapes the cylinder and is available in the exhaust manifold to be recovered[1]. This high pressure and temperature gas can be expanded in a turbine to drive a compressor, leading to higher engine power densities and lower fuel consumption and emissions. However, the application of this technology requires the study of coupling strategies between the engine and the turbocharger, being the variable geometry turbine (VGT) the most extended solution in diesel applications. Although it is difficult to use a VGT with a petrol engine due to the high exhaust temperatures, it is currently being evaluated as a very attractive way of driving down emissions and fuel consumption also in these engines, as described in[2].

Most of the fluid-dynamic processes that take place in the engine can be reproduced by means of zero-dimensional and simple one-dimensional models, providing reasonable precision with very low computational cost. In this context, using mainly the characteristic curves could be the most efficient solution. Nevertheless, that implies using information of previous measurements to characterise the curves in an operating range that is usually wider that the one provided by manufacturers. In addition, it makes mandatory to interpolate and makes impossible to extrapolate or to consider mass accumulation during unsteady operation.

For that reason, the correct physical modelling of the variable geometry turbine, with an evolved one-dimensional model, provides a powerful tool for the analysis and development of reciprocating engines, and in particular, valuable information for the design of the necessary matching between engine and turbocharger plus the required control strategies. Active control systems such as the one described by Pesidiris[3] can also be implemented more easily with more accurate pulsating flow simulations. Furthermore, better predictions in the turbine outlet line can lead to a better design of the aftertreatment and silencer, and, consequently, to an improvement in the consumption and pollutant emissions.

A lot of improvements have been seen in this area during the last decade, as shown in the works by Romagnoli et al.[4] or Payri et al.[5]. Furthermore, some advances developed in the classic unidimensional approach can be found in the works of Chen et al.[6], Costall et al.[7] or De Bellis et al.[8]. Other aspects of the turbocharger behaviour can be taken into account in these simulations. Such is the case of the heat transfer effects, that can be determined experimentally with a simple lumped model as in[9] or[10]. The simplifications that are used in simple turbocharger heat transfer models that are coupled with one-dimensional gas dynamics codes have been validated both experimentally and with computational fluid dynamics (CFD) simulations, as in[11]. The results of including a heat transfer model to determine internal heat flows has been investigated by several authors, such as in the works by Olmeda et al.[12] or Serrano et al.[13]. These models can even be used to obtain information that is difficult to measure in an experiment, such as the difference heat flow paths, as in the work by Aghaali et al.[14]. Friction losses models as the one developed by Serrano et al.[15] or Marelli et al.[16] have been also coupled with one-dimensional gas dynamics codes so the mechanical efficiency can be computed in time marching simulations, as shown in[17]. Several works about radial turbine modelling can be found in the literature, where the properties of the internal flow of the turbine under different boundary conditions are presented and discussed, as can be seen in the works by Galindo et al.[18,19] and Hakeem et al.[20]. Especially focused in the unsteady performance at high frequencies are the works by Hu[21] and King[22]. Also, the experimental characterisation of turbochargers is increasing in complexity in parallel to the models that use this information. This can be seen in the works by Rajoo et al.[23] or Hohenberg et al.[24] for pulsating flow in

[1]CMT - Motores Térmicos, Universitat Politècnica de València, ES

Corresponding author:
Luis Miguel García-Cuevas, CMT - Motores Térmicos, Universitat Politècnica de València, Camino de Vera, Valencia 46022, Spain
Email: luiga12@mot.upv.es

turbines, Serrano et al.[25] for off-design performance of turbines or Torregrosa et al.[26], Leufvén and Eiriksson[27] and Galindo et al.[28] for the performance, including noise emissions and off-design working conditions, of radial compressors.

In this work, a quasi-bidimensional approximation is proposed with the intention of improving the current performance at high frequencies of the equivalent one-dimensional duct approach with the minimal penalty in computational costs.

The objectives of this paper are to present a method to get pressure data in a radial turbine and to fit and validate a simple quasi-two-dimensional turbine model, derived from[29], with that experimental data. This model is able to take into account the circumferential non-uniformity of the flow at the volute outlet section, which is an important feature to capture the high-frequency performance of the turbine, as shown by Ding et al.[30].

The paper is structured as follows: first, a very simple description of the model is shown and its calibration method is described; second, the experimental setup is explained; third, the model is compared with the experimental data and the main results are discussed; finally, the main conclusions are presented.

Model description and calibration

In this section, the main aspects of the model will be described and the calibration method will be presented, including the main experimental data needed during the fitting procedure and validation. It is important to mention that the model presented in this paper is an evolution of a pure 1D model, described in[6] and sketched in Figure 1. Section 0 represents the domain inlet section, section 1 is turbine inlet, section 2 is the equivalent stator nozzle, section 3 is the rotor inlet, section 4 is the rotor outlet, section 5 is the turbine outlet and section 6 is the domain outlet.

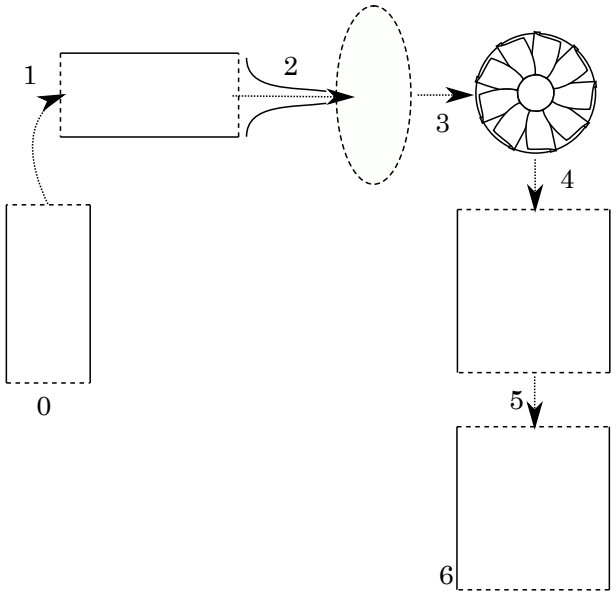

Figure 1. Previous 1D Model. The main sections are labeled with numbers.

Model description

The model is divided in several parts: one-dimensional flow ducts (turbine inlet and outlet) and a quasi-bidimensional duct (volute). The stator and the rotor are modelled as equivalent nozzles and are computed using variable equivalent areas and a virtual plenum between them. The model schematic is shown in Figure 2, where the same numbering for the different sections is used as in the case of the pure 1D model.

The one-dimensional elements, such as the turbine inlet and outlet ducts, are discretised by means of a finite-volume approach and computed using a Godunov scheme, as first described in the work by the mentioned author[31]. For that purpose, a Riemann-solver (see[32]) has been employed. In order to improve the spatial accuracy of the integration, a second order Monotone Upstream-centered Schemes for Conservation Laws (MUSCL) scheme has been used (see[33]). The time-step is chosen at each integration step in order to obey the Courant-Friedrichs-Lewy (CFL) condition[34].

In the case of the volute, the same methodology has been applied but taking into account that, although the volute is simulated as a one dimensional tapered duct, source terms will be considered in the 1D conservation equations due to the flow leaving through the lateral window. The addition of these source terms, computed using the stator results, allows the model to capture the non-uniformity of the flow in the volute during the pulse transmission. A more realistic volute geometry is used in this case: instead of a simple straight duct with half of the actual turbine length, the real section distribution and length are used.

The source term $\dot{m}_{\mathrm{cell}}$ for the mass conservation equation for a volute cell is shown in Equation 1:

$$\dot{m}_{\mathrm{cell}} = \dot{m}_{\mathrm{st}} \tag{1}$$

where $\dot{m}_{\mathrm{st}}$ is the mass flow that passes through one of the stator channels, using as total inlet conditions the total pressure and temperature of the volute cell, and is computed as described in the following paragraphs. The source term $\dot{H}_{\mathrm{cell}}$ for the energy conservation equation for a volute cell is shown in Equation 2:

$$\dot{H}_{\mathrm{cell}} = \dot{m}_{\mathrm{st}} \cdot c_{\mathrm{p}} \cdot T_{\mathrm{cell,t}} \tag{2}$$

where c_{p} is the isobaric specific heat capacity and $T_{\mathrm{cell,t}}$ is the total temperature of the cell. Finally, the source term $\dot{q}_{\mathrm{cell}}$ for the momentum conservation equation is computed as in Equation 3:

$$\dot{q}_{\mathrm{cell}} = \dot{m}_{\mathrm{st}} \cdot v_{\mathrm{cell}} \tag{3}$$

where v_{cell} is the axial flow velocity in the cell.

Regarding the prediction of the flow variation around the volute, the work by Chiong et al.[35] proposes a different solution based on a non-adiabatic pressure loss boundary condition. Also in[29], a description of the quasi-bidimensional model of the volute can be found, however, the stator and rotor are not modelled as it is presented in this paper, as it will be explained next.

The stator is solved as several nozzles connected to the volute, each to a volute cell, and to the stator outlet discharge zone using several equivalent effective areas. This way, the non-uniformity of the flow properties in the volute outlet section can be taken into account. On the other hand, the rotor is modelled using one equivalent nozzle with a determined equivalent effective area. Once the effective areas are known, the computation of the real flow through the stator and through the rotor is easily obtained by considering adiabatic behaviour in the nozzles. The procedure to obtain these effective areas is described in the calibration subsection.

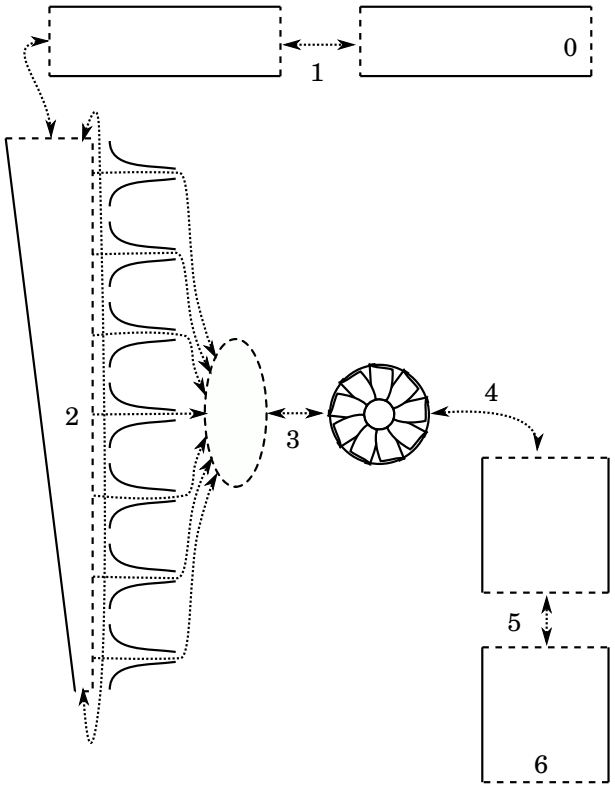

Figure 2. Q2D Model schematic. The main sections are numbered.

In order to simplify the validation process, the flow evolution is supposed to be adiabatic, so quasi-adiabatic experimental data is needed. Some basic geometrical data will also be necessary. The following geometrical data is used by the proposed model:

- Ducts and volute lengths and section distribution.
- Stator blades sizes and positions.
- Stator inlet and outlet radii and height.
- Rotor outlet tip and nut radii.
- Rotor outlet metal angle.

The volute itself has been used as a mould in which silicone has been injected in order to get its geometry. After the silicone had cured, it was extracted and measured. The mould can be seen in Figure 3.

After that, several photographs were taken and a vernier calliper used to measure the rotor diameters and the rotor outlet angle, as portrayed in Figure 4. The inlet and outlet wheel diameter are 41 mm and 38 mm respectively.

Finally, more photographs where taken to measure the position of the stator vanes, their lengths and angles for different VGT displacements. The angle of each vane was individually measured and their mean value was used for each VGT displacement.

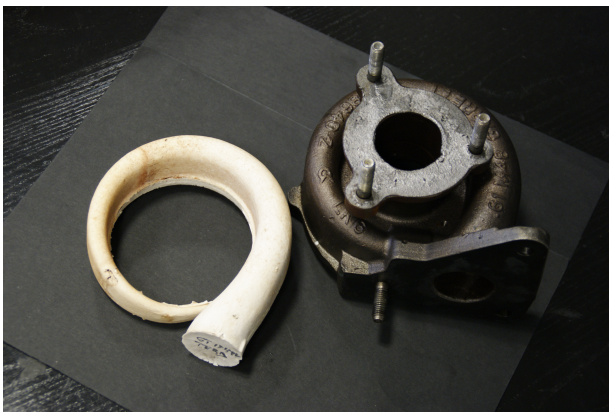

Figure 3. A silicone mould of the volute.

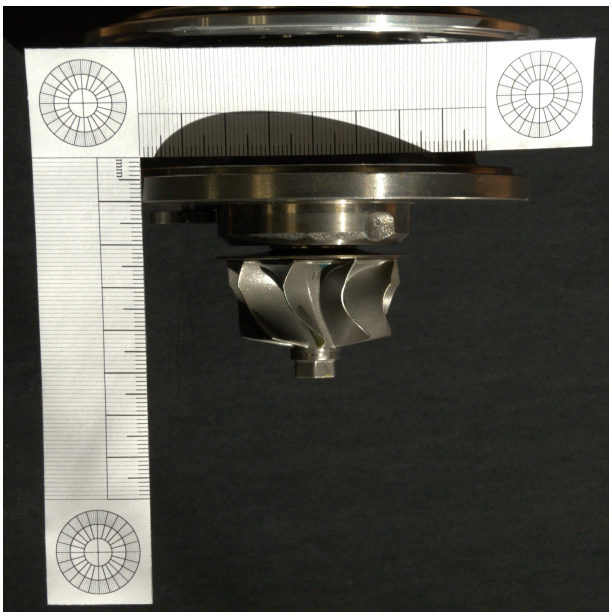

Figure 4. The turbine rotor wheel.

Calibration method

In this subsection, the model fitting will be described in detail along with the equations that are needed. To succeed in the fitting process, turbine mass flow rate, inlet total conditions and stator static pressure during steady tests must be measured.

Firstly, to capture the unsteady phenomena in any engine working condition, the model needs information of the reduced mass flow and the adiabatic efficiency in the complete turbine operation range. To achieve that, an extrapolation procedure described in detail in[36] and based on modelling the turbine as a single equivalent nozzle is approached. This method, which is able to extrapolate the radial turbine performance in terms of VGT position, rotational speed and blade speed

ratio, uses thirteen calibration coefficients; seven for the reduced mass flow and six for the efficiency.

In the case of the reduced mass flow extrapolation procedure, the starting point is the use of continuity applied to stator, rotor and equivalent nozzle as shown in Equation 4. Regarding the equivalent nozzle area, using the velocity definition and solving the mass flow, Equation 5 is obtained, and, assuming certain hypothesis (as shown in the work by Serrano et al.[36]), a new equation of the throat area of the equivalent nozzle is deduced 6:

$$\dot{m} = A_{2'}\rho_{2'}v_{2'} = A_4\rho_4 w_4 = A_{\mathrm{Neq}}\rho_4 v_{\mathrm{Neq}} \tag{4}$$

$$A_{\mathrm{Neq}} = A_4\sqrt{\frac{1+\left(\frac{u_4}{v_{\mathrm{Neq}}}\right)^2-\left(\frac{u_3}{v_{\mathrm{Neq}}}\right)^2+\left(\frac{w_3}{v_{\mathrm{Neq}}}\right)^2}{\left(\frac{A_4}{A_{2'}}\right)^2\left(\frac{\rho_4}{\rho_{2'}}\right)^2+1}} \tag{5}$$

$$A_{\mathrm{Neq}} = \frac{a\cdot A_4\cdot\sqrt{1+\frac{\sigma^2\cdot\left[\left(\frac{D_4}{D_3}\right)^2-1\right]+b}{\bar{\eta}_{\mathrm{t,s}}}}}{\sqrt{1+\left(c\cdot\frac{A_4}{A_{2'}}\right)^2\cdot\frac{\left(\frac{1}{\pi_{2',4}}\right)^2}{\left\{1-\eta_{\mathrm{t,s}}\cdot\left[1-\left(\frac{1}{\pi_{2',4}}\right)^{\frac{\gamma-1}{\gamma}}\right]\right\}^2}}} \tag{6}$$

It is important to point out that Equation 6 depends only on easy measurable geometry parameters of the turbine and on the information available in a standard map. Once the equivalent nozzle area A_{Neq} is known, the reduced mass flow can be calculated considering flow through an orifice with isentropic expansion:

$$\dot{m}_{\mathrm{red}} = A_{\mathrm{Neq}}\sqrt{\frac{\gamma}{\Re}}\left(\frac{1}{\pi_{1\mathrm{t},4\mathrm{s}}}\right)^{\frac{1}{\gamma}}\cdot\sqrt{\frac{2}{\gamma-1}\left[1-\left(\frac{1}{\pi_{1\mathrm{t},4\mathrm{s}}}\right)^{\frac{\gamma-1}{\gamma}}\right]} \tag{7}$$

On the other hand, to calculate the adiabatic efficiency in Equation 8, the Euler equation and the turbine enthalpy drop are used. Through this procedure, Equation 9 is reached. However, as proved in Serrano et al.[36], Equation 10 can be deduced, which is built with the fitting parameters.

$$\eta_{\mathrm{t,s}} = \frac{T_{1\mathrm{t}}-T_{4s}}{T_{1\mathrm{t}}-T_{4\mathrm{s,isentropic}}} \tag{8}$$

$$\eta_{\mathrm{t,s}} = -2\left(\frac{D_4}{D_3}\right)^2\sigma^2+2\frac{A_{\mathrm{Neq}}}{A_1}\left(\tan\alpha_3+\frac{D_4}{D_3}\tan\beta_4\right)\cdot\left[\frac{1}{\pi_{1\mathrm{t},4\mathrm{s}}}\right]^{\frac{1}{\gamma}}\sigma \tag{9}$$

$$\eta_{\mathrm{t,s}} = -d\sigma^2+e\left(1-\frac{f}{\sigma^2}\right)^{\frac{1}{\gamma-1}}\cdot\sigma \tag{10}$$

As a result, Equation 5 and Equation 10 can be used for the non-linear fitting process of the coefficients and they should be solved iteratively as a system, since the reduced mass flow appears in the efficiency equation and the efficiency equation appears in the reduced mass flow equation. To succeed in the fitting procedure, some boundary conditions for the coefficients must be considered, that way, the definition of each coefficient has a physical explanation. With the fulfilment of this procedure, demonstrated in[36], the radial turbine performance has been extrapolated and an effective area of the equivalent nozzle has been characterised for a wide range of operating points.

It is commonplace to consider a value for the reaction degree of $R = 0.5$ to model the behaviour of radial turbines designed without guide blades. Nevertheless, that hypothesis cannot be generally accepted when modelling variable radial turbines. For that reason, an additional procedure, detailed in[37], is applied in order to calculate the pressure drop across the turbine stator and rotor and thus, evolve the model up to two nozzles with an intermediate volume between them. In summary, the intermediate pressure can be expressed as:

$$\frac{p_3}{p_1} = \left(1+\frac{T_{1\mathrm{t}}}{T_1}(R-1)\eta_{\mathrm{t,s}}\left[1-\left(\frac{p_4}{p_{1\mathrm{t}}}\right)^{\frac{\gamma-1}{\gamma}}\right]\right)^{\frac{\gamma-1}{\gamma}} \tag{11}$$

where

$$R = 0.5 \qquad \text{if } \alpha_1 > \alpha_{\mathrm{limit}} \tag{12}$$

and

$$R = 1-\frac{2\cdot\Re}{\pi^2 D_3\left(D_4^2-D_{4,nut}^2\right)}\cdot\frac{\dot{m}_{\mathrm{red}}\cdot\tan\alpha_3}{N_{\mathrm{red}}}\cdot\left(\frac{p_4}{p_{1\mathrm{t}}}\right)^{-1}\left\{\left(\frac{T_{1\mathrm{t}}}{T_1}\right)^{-1}-\eta_{\mathrm{t,s}}\left[1-\left(\frac{p_4}{p_{1\mathrm{t}}}\right)^{\frac{\gamma-1}{\gamma}}\right]\right\} \tag{13}$$

otherwise.

Note that in the previous equations the only inputs are geometrical parameters, along with the typical variables provided by turbochargers manufacturers. Furthermore, instead of a variable polytropic coefficient, isentropic evolution has been considered in order to simplify the calculations. Once the pressure drop across the stator is calculated, the effective areas of the nozzles equivalent to the stator and the rotor can be obtained from Equation 14 and Equation 15, where $p_{1\mathrm{t,rel}}$ is the relative condition at the rotor inlet. In addition, to obtain the term $p_{1\mathrm{t,rel}}/p_2$, Equation 16 must be computed.

$$A_{\mathrm{eff,st}} = \dot{m}\cdot\frac{\sqrt{\Re\gamma T_{1\mathrm{t}}}}{p_{1\mathrm{t}}}\cdot\frac{1}{\gamma}\cdot\left(\frac{p_{1\mathrm{t}}}{p_3}\right)^{1/\gamma}\cdot\left\{\sqrt{\frac{2}{\gamma-1}\left[1-\left(\frac{p_3}{p_{1\mathrm{t}}}\right)^{\frac{\gamma-1}{\gamma}}\right]}\right\}^{-1} \tag{14}$$

$$A_{\mathrm{eff,rot}} = \dot{m}\cdot\frac{\sqrt{\Re\gamma T_{3\mathrm{t}}}}{p_{3\mathrm{t}}}\cdot\frac{1}{\gamma}\cdot\left(\frac{p_{3\mathrm{t,rel}}}{p_4}\right)^{1/\gamma}\cdot\left\{\sqrt{\frac{2}{\gamma-1}\left[1-\left(\frac{p_4}{p_{3\mathrm{t,rel}}}\right)^{\frac{\gamma-1}{\gamma}}\right]}\right\}^{-1} \tag{15}$$

$$\frac{p_{3t,rel}}{p_4} = \frac{p_3}{p_1} \cdot \frac{p_{1t}}{p_4} \cdot \left(\frac{T_1}{T_{1t}}\right)^{\frac{\gamma}{\gamma-1}} \cdot \left[\left(1 + \left(\frac{T_{1t}}{T_1} - 1\right) \cdot \frac{T_1}{T_3}\right]^{\frac{\gamma}{\gamma-1}} \quad (16)$$

Finally, with the rotor and stator equivalent areas, the mass flow can be obtained taking into account that the total temperature is conserved when considering isentropic nozzle flow. Again, the explanation of the hypotheses and the demonstrations of the previous equations can be found in [37].

Experimental setup

The experiments have been done in a turbocharger gas stand with the following arrangement:

- A screw compressor with a maximum flow rate of 0.2 kg s^{-1} and a maximum discharging absolute pressure of 0.4 MPa provides the mass flow to the turbine. This mass flow rate is controlled by the screw compressor speed and an electronic discharge valve placed after the screw compressor. The discharge valve is used when a very small mass flow rate and turbine inlet pressure is required.
- The temperature of the flow that goes to the turbine can be controlled:
  - Cooled by a water-air heat exchanger.
  - Heated by five electrical heaters with an installed power of 40 kW, rising the turbine inlet temperature up to 720 K at maximum flow rate.
- The flow that enters the turbocharger compressor passes through a filter and a water-air heat exchanger in order to regulate the compressor inlet temperature.
- The turbocharger compressor flow is controlled by means of a backpressure valve.
- The compressor side of the gas stand can be operated in closed-loop, so the flow can be pressurised. This leads to wider operating ranges when using the turbocharger compressor as a braking system while measuring turbine maps.
- A rotary valve can be placed upstream of the turbine or downstream of the compressor to generate pulses similar to that found in a reciprocating engine.
- An independent lubrication system is used for the turbocharger. The oil pressure and temperature can be adjusted for each experimental test.
- A hot film flow meter is placed at the turbine side gas stand outlet, after a water-air heat exchanger. This mass flow meter has an expanded uncertainty of 2 % of the measured value in the worst case for the measured values during the experimental campaign.
- Type K thermocouples, with an expanded uncertainty of 1.5 K per thermocouple, are used to measure air temperatures at the turbine inlet and outlet in all the experimental tests.
- Piezoresistive transmitters are used to measure the static air pressure at the turbine inlet and outlet.
- Three piezoresistive transducers are used to measure instantaneous static pressure at the turbine inlet and outlet.
- An induced currents transducer is placed at the compressor side to monitor the turbocharger speed.
- A displacement transducer is used to measure the VGT position. The maximum opening corresponds to a VGT position of 100 % and the minimum to 0 %. Using the straight-line method all the intermediate positions are known.
- All the sensors are installed according to Society of Automotive Engineers (SAE) J1723 and J1826 standards [38,39].

In Figure 5 the gas stand schematic used during the tests is presented. The internal cooling system (ICS) and the internal lubrication system (ILS) are also provided with pressure and temperature sensors, along with mass flow sensors, but they have been omitted for clarity's sake.

The heat flow has been maintained as low as possible during the experimental campaign, in what is commonly called quasi-adiabatic conditions. To ensure it, the turbine and lubrication inlet temperatures have been set to be close to the compressor outlet temperature, with a maximum allowed discrepancy of ±6 K and a mean value of ±2.5 K. Also, as the compressor outlet temperature is relatively low and the ducts were thermally insulated, the heat flow to the environment is bounded to a small amount of around 2 % of the measured turbine power output, as can be seen in Figure 6. This heat flow to the environment has been estimated using the environment temperature T_{env}, the maximum surface temperature of the turbine T_{surf} and the exposed surface of the ducts and turbine A_{surf}, and assuming a convective heat transfer coefficient h_{conv} of 10 W m^{-2} K^{-1}:

$$\dot{Q}_{env} = A_{surf} \cdot h_{conv} \cdot (T_{surf} - T_{env}) \quad (17)$$

The turbine power output is estimated using the total enthalpy flow as follows:

$$\dot{W} = \dot{m} \cdot c_p \cdot (T_{6t} - T_{0t}) - \dot{Q}_{int} \quad (18)$$

where the term $\dot{Q}_{int}$ corresponds to the internal heat losses from the gas to the turbine shroud, and is calculated as described in [10].

In the next figure is shown the expected error in percentage in the calculation of the turbine power output due to the external heat losses.

Experimental campaign details

The experimental campaign consisted of two clearly differentiated parts: in the first one, the turbine map was measured in quasi-adiabatic conditions; in the second one, a rotary valve was used at the turbine inlet imposing pulsating flow. The fundamental frequency of the pulses generated were 50 Hz, 66 Hz and 100 Hz, that correspond to 1500 rpm, 2000 rpm and 3000 rpm in a 4

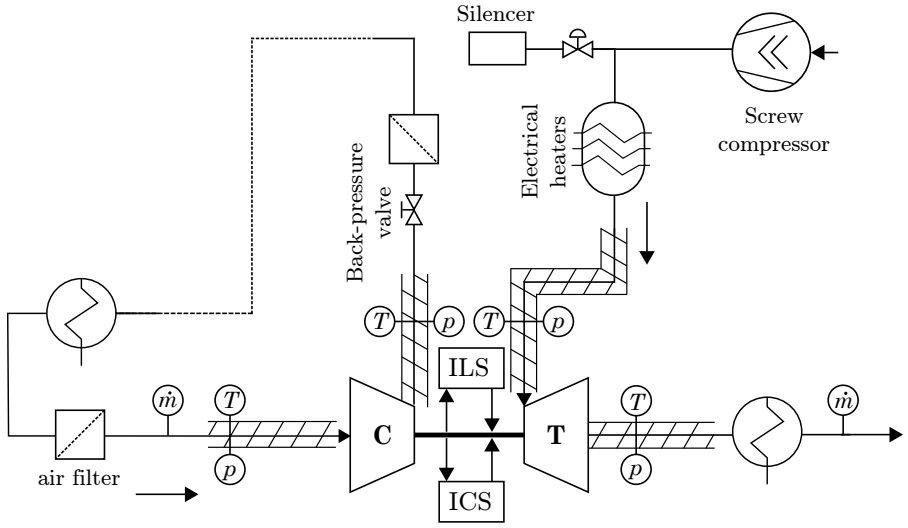

Figure 5. Gas stand schematic

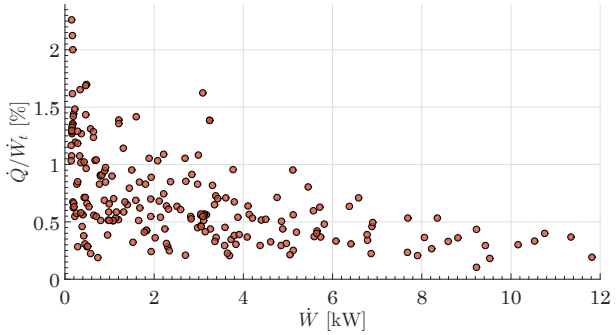

Figure 6. Expected error in turbine power output due to external heat flow effects.

cylinders 4 stroke engine. Different turbocharger speeds were evaluated in the same VGT positions that were measured during the steady flow tests:

Turbo speeds : 58 krpm, 99 krpm, 122 krpm, and 123 krpm.

VGT positions : 56 %, 80 %, 60 % and 50 %.

In the pulsating campaign , the incident and 2nd reflection waves were imposed as can be observed in Figure 7. The reflected and transmitted waves were then compared to the ones obtained from the model, using the works by Piñero et al.[40] for the pressure decomposition.

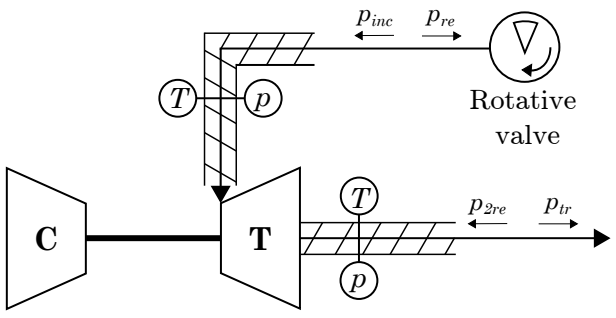

Figure 7. Pulsating test schematic. Incident and 2nd reflection waves are imposed.

Different pressure and temperature sensors where placed at the same radial position but different azimuths, with differences in the range of a few kPa and less than one K. As the measurement uncertainty was of the same order, their mean value was used for the calibration and validation phase.

Results

The results for the turbine map can be seen in Figure 8 and Figure 9. The markers represent the experimental points, whereas the lines represent the model results. It is worth noting that only five points per speed line were used to calibrate the model. Only a small fraction of the points are shown in Figure 9 for clarity's sake. The model has been fitted using the procedure described in section 'Calibration method' using a random subset of one half of the measured points. The turbine reduced mass flow rate $\dot{m}^*$ and power output $\dot{W}$ are plotted against the turbine total to static expansion ratio $\pi_{0t,6}$. The turbine reduced mass flow rate is defined as:

$$\dot{m}^* = \dot{m} \cdot \frac{\sqrt{T_{0t}}}{p_{0t}} \tag{19}$$

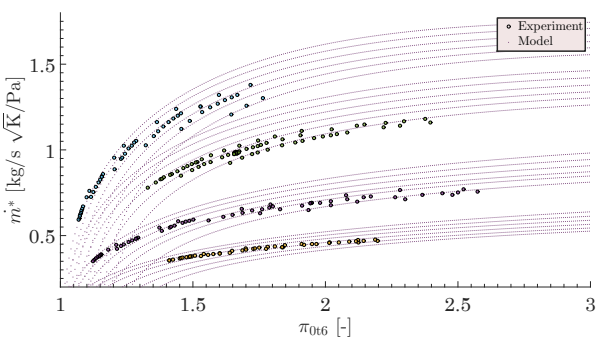

Figure 8. Turbine map - measured vs. model.

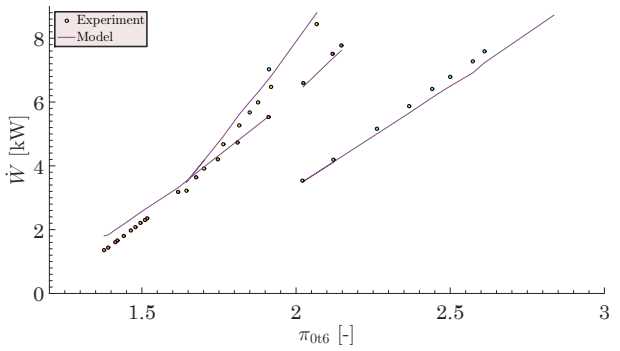

Figure 9. Turbine map, power output - measured vs. model.

The instantaneous simulations were carried out imposing the incident wave in the inlet and the 2nd reflection wave in the outlet. In order to obtain the incident, reflected, transmitted and 2nd reflection from the composed pressure, Beamforming techniques have been used[40].

An example of the results can be seen from Figure 10 to Figure 13, where the power spectral density of the static pressure is plotted at two different points; the turbine domain inlet (inlet pipe, position 0), and the turbine domain outlet (outlet pipe, position 6) for four different working conditions. The figures also show the instantaneous air mass flow in the time domain, for the same working points at the same locations. The experimental results are plotted against the values provided by the 1D classic volute model and the quasi-bidimensional model. The power spectral density is computed using Welch's average periodogram method[41] using a Hann window[42] with a 50 % overlap. Results are presented for excitations of 66 Hz and 100 Hz, corresponding to 1500 and 3000 rpm, nevertheless, the models have been validated for several other excitations.

Both in the air mass flow and in the pressure results the two models present similar behaviour in the time domain so, in order to study the differences between them, the attention should be focused in the frequency domain results. Although both models present some differences with the experimental data, the quasi-bidimensional volute presents better fidelity with the experimental results in the range from 1000 Hz to 2000 Hz mainly due to the "averaging" effect as the flow exits through its lateral window. In particular, it can be observed that the 1D volute model tends to overestimates the values in the high frequency range.

From the results it can be inferred that the improvement of the Q2D model is slightly more evident where the pulses have a higher fundamental frequency. This can be explained by the fact that in the higher engine speed cases (higher fundamental frequencies) the wave length reaches the volute length order of magnitude at lower order and higher amplitude harmonics than in the low engine speed cases. Nevertheless, no significant trends were found in terms of VGT position.

Regarding the turbine efficiency comparison, experimental instantaneous efficiency is not available and thus, only the pulse-average efficiency for both modelling approaches is presented (see Figure 14). In addition, the expanded uncertainty of this measurement (with a coverage factor of 3 and in red in Figure 14) is in the order of magnitude of the difference presented between the different models and so, it would be risky to obtain any trend or conclusion. For future experimental campaigns it will be crucial to be able to obtain the instantaneous efficiency and compare both model approaches against these new data.

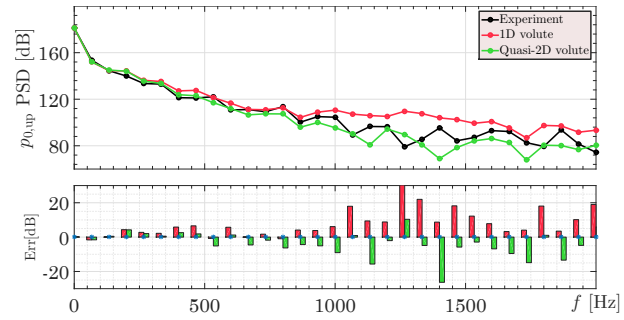

(a) Reflected pressure, PSD

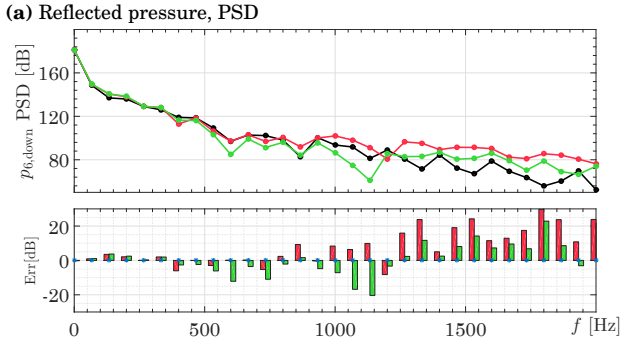

(b) Transmitted pressure, PSD

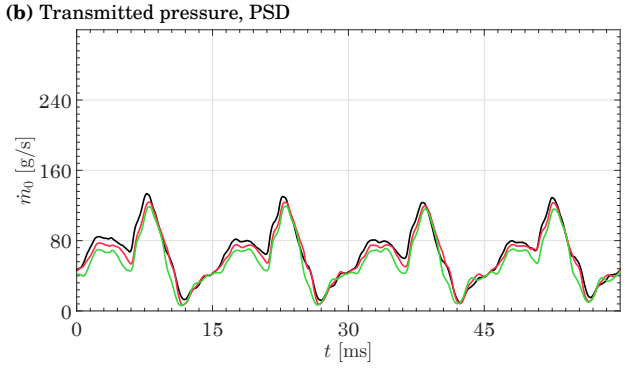

(c) Turbine inlet mass flow rate

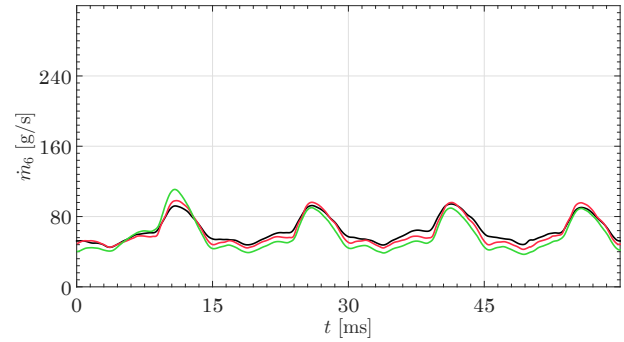

(d) Turbine outlet mass flow rate

Figure 10. VGT at 56 %, 58 krpm, 66.7 Hz.

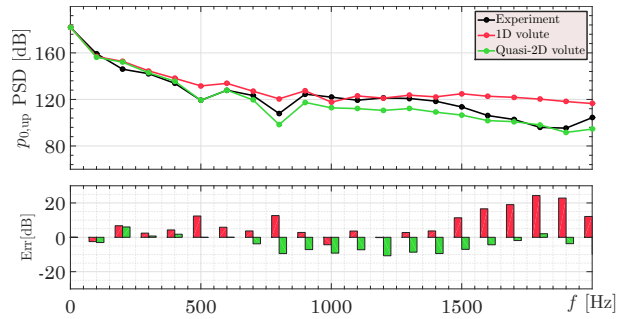

(a) Reflected pressure, PSD

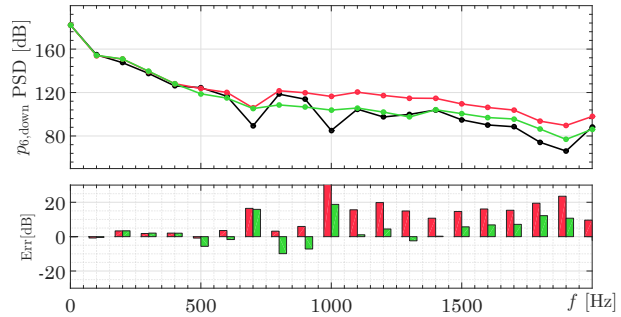

(b) Transmitted pressure, PSD

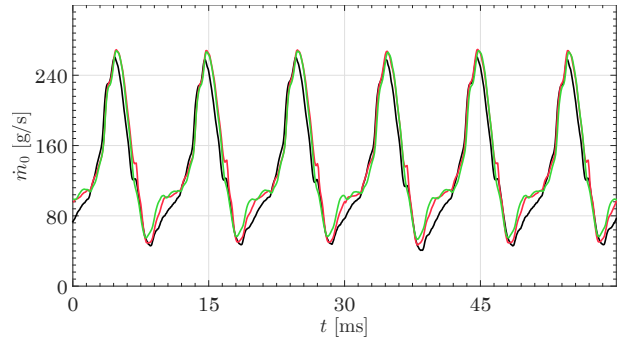

(c) Turbine inlet mass flow rate

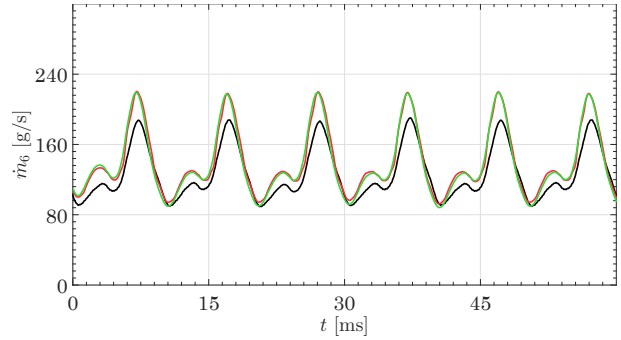

(d) Turbine outlet mass flow rate

Figure 11. VGT at 80 %, 99 krpm, 100 Hz.

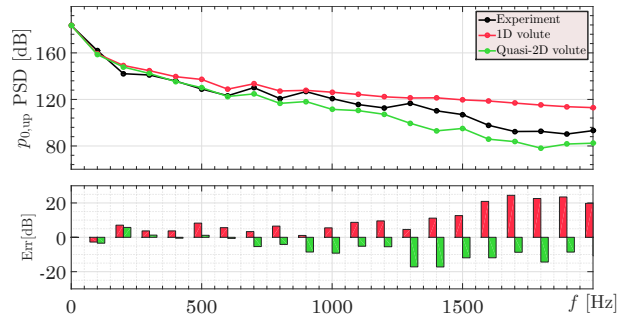

(a) Reflected pressure, PSD

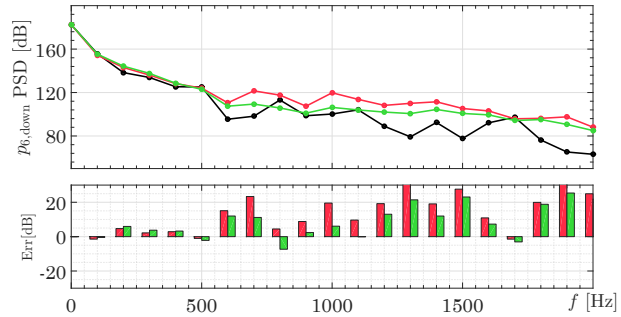

(b) Transmitted pressure, PSD

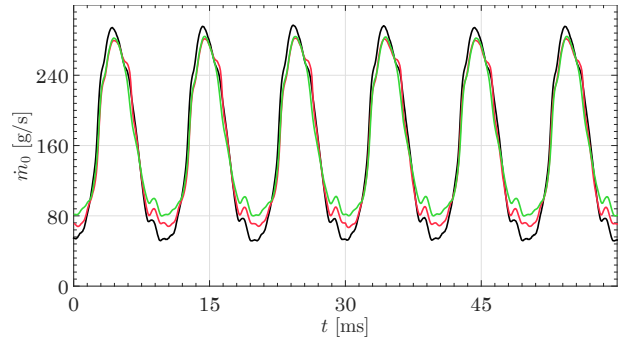

(c) Turbine inlet mass flow rate

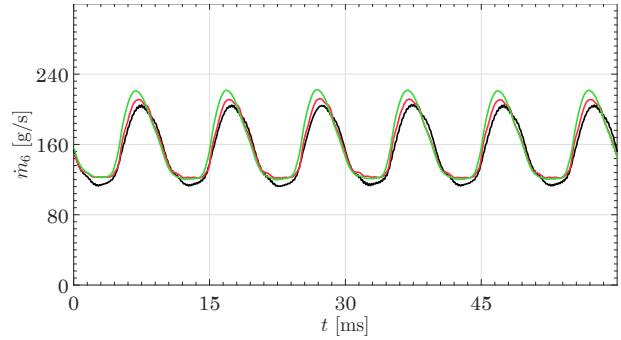

(d) Turbine outlet mass flow rate

Figure 12. VGT at 60 %, 122 krpm, 100 Hz.

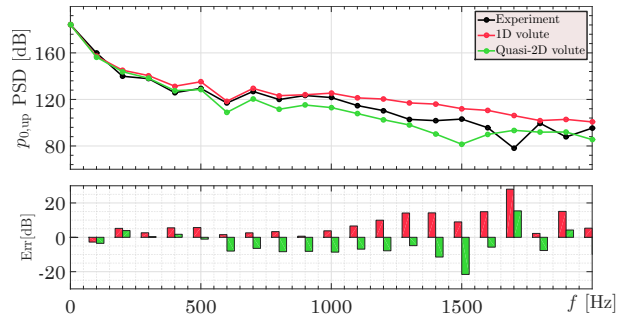

(a) Reflected pressure, PSD

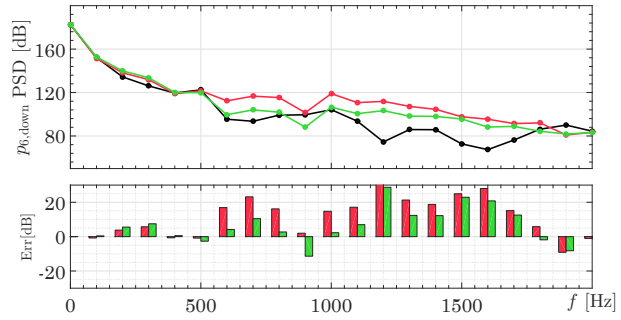

(b) Transmitted pressure, PSD

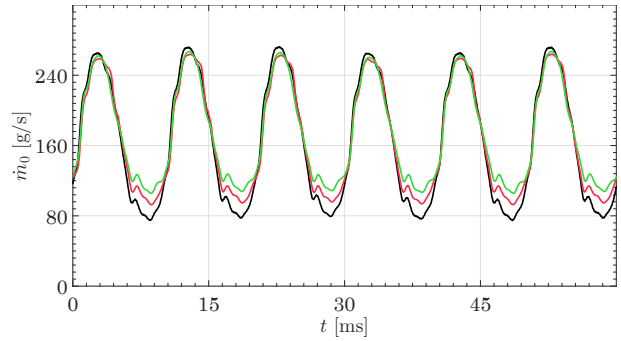

(c) Turbine inlet mass flow rate

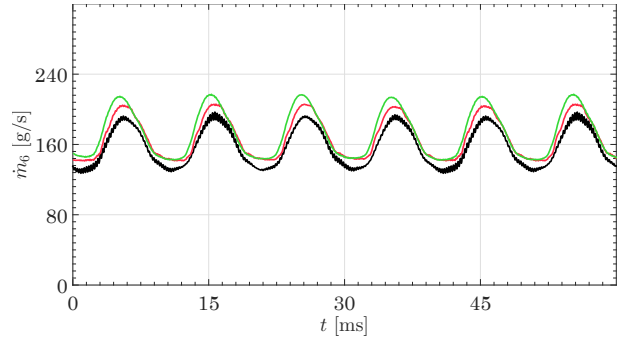

(d) Turbine outlet mass flow rate

Figure 13. VGT at 50 %, 123 krpm, 100 Hz.

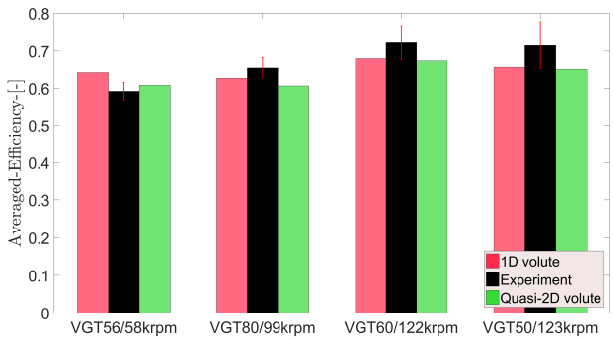

Figure 14. Turbine pulse-average efficiency

Conclusions

In this paper, a method to measure the pressure of a radial turbine under continuous and pulsating flow conditions is presented. The experimental results obtained are used to fit and validate a quasi-two-dimensional model and to compare it with the classic one-dimensional model.

The pulsating flow conditions are generated by means of a rotating valve placed upstream of the turbine, designed in a way that would approximate the behaviour of that found in the exhaust manifold of a four cylinder, four strokes reciprocating engine. Furthermore, piezoelectric transducers are placed in the turbine inlet and outlet lines for beamforming purposes. That way, relevant experimental information about pulsating conditions in a wide range of turbocharged engine operating points has been obtained, in particular, incident and reflected waves for the turbine inlet and transmitted and second reflection waves for the turbine outlet can be analysed.

The quasi-two-dimensional model has proven to be an appropriate method to improve the previous one-dimensional duct approaches, especially at high frequencies. The classic volute model produces good predictions at up to 1000 Hz, while the new model improves these results and obtained better predictions at up to 2000 Hz. Contrary to what occurs in the fully one-dimensional model, in the quasi-two-dimensional volute different stator channels are exposed to different inlet condition. In this manner, the volute produces an averaging effect in the pressure pulse at high frequencies that reduces the amplitude of the signal and can't be reproduced using a one-dimensional duct. Higher frequencies remain out of the scope of this study, as they are affected by flow phenomena that is neither simulated nor modelled, so it could only be properly reproduced with further development of the model. This improvement in the accuracy of the results comes with a slight increment of the computational cost, in particular, the additional source term must be computed for each volute cell and around twice the number of volute cells are used so, as a result, for the same cell size, the quasi-2D approach doubles the time while computing the volute element.

It is worth mentioning that a better prediction of the conditions in the turbine line can be crucial for obtaining a more optimized design of the silencer

and aftertreatment systems. This affects the pumping losses so the total fuel consumption and the pollutant emissions will be affected as well. Furthermore, a different design implies different back pressure and, in consequence, different turbocharger matching.

Nowadays, one-dimensional and zero-dimensional models of full engines are fast enough to be implemented in real-time simulations such as hardware-in-the-loop (HIL) with an acceptable but also improvable precision. Thus, in the following years, maintaining low computational costs in the turbocharger code will be crucial, specially considering that the development and the application of these systems are becoming more and more essential in the engine research field. Furthermore, the quasi-two-dimensional model should be also trivially adapted to twin-entry and waste-gate turbines, such as the ones used in petrol engines.

Acknowledgements

Pablo Soler is partially supported through contract FPI-2017-S2-1428 of Programa de Apoyo para la Investigación y Desarrollo (PAID) of Universitat Politècnica de València. The authors of this paper wish to thank M.A. Ortiz and V. Ucedo for their invaluable work during the experimental setup and the campaign.

List of symbols

A	Area
a	First fitting parameter for A_{Neq}
b	Second fitting parameter for A_{Neq}
c	Third fitting parameter for A_{Neq}
c_{p}	Specific heat capacity at constant pressure
D	Diameter
d	First fitting parameter for the efficiency
e	Second fitting parameter for the efficiency
f	Third fitting parameter for the efficiency
$\dot{H}$	Energy source term
h	Heat transfer coefficient
$\dot{m}$	Mass flow rate
p	Pressure
$\dot{Q}$	Heat flow
$\dot{q}$	Momentum source term
R	Reaction degree
$\Re$	Gas constant
T	Temperature
t	Time
u	Blade tip speed
v	Absolute speed
w	Relative speed
$\dot{W}$	Power

Greek letters

α	Absolute flow angle
β	Relative flow angle
η	Efficiency
γ	Heat capacities ratio
π	Pressure ratio
ρ	Density
σ	Blade speed ratio

Subscripts and superscripts

0	Gas stand inlet section
1	Turbine inlet section
2	Volute lateral window section
2'	Nozzle throat section
2re	Second reflection
3	Rotor inlet section
4	Rotor outlet section
5	Turbine outlet section
6	Gas stand outlet section
cell	Volute cell
conv	Convection
down	Downstream travelling wave
eff	Effective
env	Environment
inc	Incident wave
isentropic	Isentropic conditions
limit	Limit value
Neq	Equivalent nozzle
nut	Wheel nut
up	Upstream-travelling wave
re	Reflected wave
red	Reduced quantity
rel	Relative reference frame
rot	Rotor
s	Static conditions
st	Stator
surf	Surface
t	Total conditions
tr	Transmitted wave
$\bar{}$	Mean value
*	Reduced value

Acronyms

CFL	Courant-Friedrichs-Lewy condition
ICE	Internal combustion engine
ICS	Independent cooling system
ILS	Independent lubrication system
MUSCL	Monotone Upstream-centered Schemes for Conservation Laws
PSD	Power spectral density
VGT	Variable geometry turbine

References

1. Kesgin U. Effect of turbocharging system on the performance of a natural gas engine. *Energy Conversion and Management* 2005; 46(1): 11 – 32. DOI:10.1016/j.enconman.2004.02.006.
2. Tang H, Pennycott A, Akehurst S et al. A review of the application of variable geometry turbines to the downsized gasoline engine. *International Journal of Engine Research* 2015; 16(6): 810–825. DOI:10.1177/1468087414552289.

3. Pesiridis A. The application of active control for turbocharger turbines. *International Journal of Engine Research* 2012; 13(4): 385–398. DOI:10.1177/1468087411435205.
4. Romagnoli A and Martinez-Botas R. Performance prediction of a nozzled and nozzleless mixed-flow turbine in steady conditions. *International Journal of Mechanical Sciences* 2011; 53(8): 557 – 574. DOI:10.1016/j.ijmecsci.2011.05.003.
5. Payri F, Serrano JR, Fajardo P et al. A physically based methodology to extrapolate performance maps of radial turbines. *Energy Conversion and Management* 2012; 55(0): 149 – 163. DOI:10.1016/j.enconman.2011.11.003.
6. Chen H and Winterbone D. A method to predict performance of vaneless radial turbine under steady and unsteady flow conditions. In *Proceedings of IMechE 4th International Conference on Turbo-chargers and turbocharging*. Mechanical Engineering Publications, London, pp. 13–22. 1990.
7. Costall AW, McDavid RM, Martínez-Botas RF et al. Pulse performance modelling of a twin-entry turbocharger turbine under full and unequal admission. In *Proceedings of ASME Turbo Expo 2009*. ASME. DOI:10.1115/1.4000566.
8. De Bellis V and Marelli S. One-dimensional simulations and experimental analysis of a wastegated turbine for automotive engines under unsteady flow conditions. *Proceedings of the Institution of Mechanical Engineers, Part D: Journal of Automobile Engineering* 2015; 229(13): 1801–1816. DOI:10.1177/0954407015571672.
9. Bohn D, Moritz N and Wolff M. Conjugate flow and heat transfer investigation of a turbo charger: Part ii — experimental results. In *Proceedings of ASME Turbo Expo 2003*. 3686, ASME. DOI:10.1115/GT2003-38449.
10. Serrano JR, Olmeda P, Páez A et al. An experimental procedure to determine heat transfer properties of turbochargers. *Measurement Science and Technology* 2010; 21(3): 035109. DOI:10.1088/0957-0233/21/3/035109.
11. Burke R, Copeland C, Duda T et al. Lumped capacitance and three-dimensional computational fluid dynamics conjugate heat transfer modeling of an automotive turbocharger. *Journal of Engineering for Gas Turbines and Power* 2016; 138(9). DOI:10.1115/1.4032663.
12. Olmeda P, Dolz V, Arnau FJ et al. Determination of heat flows inside turbochargers by means of a one dimensional lumped model. *Mathematical and Computer Modelling* 2013; 57(7-8): 1847 – 1852. DOI:10.1016/j.mcm.2011.11.078.
13. Serrano JR, Olmeda P, Arnau FJ et al. Importance of heat transfer phenomena in small turbochargers for passenger car applications. *SAE Int J Engines* 2013; 6(2): 716 – 728. DOI:10.4271/2013-01-0576.
14. Aghaali H, Ångström HE and Serrano JR. Evaluation of different heat transfer conditions on an automotive turbocharger. *International Journal of Engine Research* 2015; 16(2): 137–151. DOI:10.1177/1468087414524755.
15. Serrano JR, Olmeda P, Tiseira A et al. Theoretical and experimental study of mechanical losses in automotive turbochargers. *Energy* 2013; 55(0): 888 – 898. DOI:10.1016/j.energy.2013.04.042.
16. Marelli S, Gandolfi S and Capobianco M. Experimental and numerical analysis of mechanical friction losses in automotive turbochargers. SAE Technical Paper 2016-01-1026, SAE International, 2016. DOI:10.4271/2016-01-1026.
17. Serrano JR, Olmeda P, Tiseira A et al. Importance of mechanical losses modeling in the performance prediction of radial turbochargers under pulsating flow conditions. *SAE Int J Engines* 2013; 6(2): 729 – 738. DOI:10.4271/2013-01-0577.
18. Galindo J, Fajardo P, Navarro R et al. Characterization of a radial turbocharger turbine in pulsating flow by means of CFD and its application to engine modeling. *Applied Energy* 2013; 103(0): 116 – 127. DOI:10.1016/j.apenergy.2012.09.013.
19. Galindo J, Hoyas S, Fajardo P et al. Set-up analysis and optimization of CFD simulations for radial turbines. *Engineering Applications of Computational Fluid Mechanics* 2013; 7(4): 441–460. DOI:10.1080/19942060.2013.11015484.
20. Hakeem I, Su CC, Costall A et al. Effect of volute geometry on the steady and unsteady performance of mixed-flow turbines. In *Proceedings of the Institution of Mechanical Engineers Part A-Journal of Power and Energy*, volume 221. pp. 535–550. 2007. DOI:10.1243/09576509JPE314.
21. Hu X. *An advanced turbocharger model for the internal combustion engine*. PhD Thesis, Purdue University, 2000.
22. King A. *A turbocharger unsteady performance model for the GT-Power internal combustion engine simulation*. PhD Thesis, Purdue University, 2002.
23. Rajoo S and Martinez-Botas RF. Variable geometry mixed flow turbine for turbochargers: An experimental study. *International Journal of Fluid Machinery and Systems* 2008; 1(1): 155–168. DOI:10.5293/IJFMS.2008.1.1.155.
24. Hohenberg KG, Newton PJ, Martinez-Botas R et al. Development and experimental validation of a low order turbine model under highly pulsating flow. In *Proceedings of ASME Turbo Expo 2017*. DOI:10.1115/GT2017-63983.
25. Serrano J, Tiseira A, García-Cuevas L et al. Radial turbine performance measurement under extreme off-design conditions. *Energy* 2017; 125: 72–84. DOI:10.1016/j.energy.2017.02.118.
26. Torregrosa AJ, Broatch A, Navarro R et al. Acoustic characterization of automotive turbocompressors. *International Journal of Engine Research* 2015; 16(1): 31–37. DOI:10.1177/1468087414562866.
27. Leufvén O and Eriksson L. Measurement, analysis and modeling of centrifugal compressor flow for low pressure ratios. *International Journal of Engine Research* 2016; 17(2): 153–168. DOI:10.1177/1468087414562456.
28. Galindo J, Tiseira A, Navarro R et al. Effect of the inlet geometry on performance, surge margin and noise emission of an automotive turbocharger compressor. *Applied Thermal Engineering* 2017; 110: 875–882. DOI:10.1016/j.applthermaleng.2016.08.099.
29. Galindo J, Tiseira A, Fajardo P et al. Development and validation of a radial variable geometry turbine model for transient pulsating flow applications. *Energy Conversion and Management* 2014; 85: 190 – 203. DOI:10.1016/j.enconman.2014.05.072.

30. Ding Z, Zhuge W, Zhang Y et al. A one-dimensional unsteady performance model for turbocharger turbines. *Energy* 2017; DOI:10.1016/j.energy.2017.04.154.
31. Godunov SK. A difference scheme for numerical solution of discontinuous solution of hydrodynamic equations. *Matematicheskii Sbornik* 1959; 47: 271–306.
32. Toro E, Spruce M and Speares W. Restoration of the contact surface in the HLL-Riemann solver. *Shock Waves* 1994; 4(1): 25–34. DOI:10.1007/BF01414629.
33. Van Leer B. Towards the ultimate conservation difference scheme. II. monotonicity and conservation combined in a second-order scheme. *Journal of Computational Physics* 1974; 14: 361. DOI:10.1016/0021-9991(74)90019-9.
34. Courant R, Friedrichs K and Lewy H. Über die partiellen differenzengleichungen der mathematischen physik. *Mathematische Annalen* 1928; 100(1): 32–74. DOI: 10.1007/bf01448839.
35. Chiong M, Rajoo S, Romagnoli A et al. Non-adiabatic pressure loss boundary condition for modelling turbocharger turbine pulsating flow. *Energy Conversion and Management* 2015; 93: 267–281. DOI:10.1016/J.ENCONMAN.2014.12.058.
36. Serrano JR, Arnau FJ, García-Cuevas LM et al. Development and validation of a radial turbine efficiency and mass flow model at design and off-design conditions. *Energy Conversion and Management* 2016; 128: 281 – 293. DOI:10.1016/j.enconman.2016.09.032.
37. Serrano JR, Arnau FJ, Dolz V et al. A model of turbocharger radial turbines appropriate to be used in zero- and one-dimensional gas dynamics codes for internal combustion engines modelling. *Energy Conversion and Management* 2008; 49(12): 3729 – 3745. DOI:10.1016/j.enconman.2008.06.031.
38. Supercharger testing standard. SAE J1723, Society of Automotive Engineers, 1995.
39. Turbocharger gas stand test code. SAE J1826, Society of Automotive Engineers, 1995.
40. Pinero G, Vergara L, Desantes JM et al. Estimation of velocity fluctuation in internal combustion engine exhaust systems through beamforming techniques. *Measurement Science and Technology* 2000; 11(11): 1585. DOI:10.1088/0957-0233/11/11/307.
41. Welch P. The use of fast fourier transform for the estimation of power spectra: A method based on time averaging over short, modified periodograms. *IEEE Transactions on Audio Electroacoustics* 1967; 15: 70–73. DOI:10.1109/TAU.1967.1161901.
42. Harris F. On the use of windows for harmonic analysis with the discrete fourier transform. In *Proceedings of the IEEE*, volume 66. IEEE, pp. 51–83. DOI:10.1109/PROC.1978.10837.